Polymer 49 (2008) 4025–4032

Contents lists available at ScienceDirect

Polymer

journal homepage: www.elsevier.com/locate/polymer

Characterization of electrospun poly(*N*-isopropyl acrylamide) fibers

Danielle N. Rockwood [a,b], D. Bruce Chase [a,c], Robert E. Akins, Jr. [a,d], John F. Rabolt [a,b,*]

[a] Department of Materials Science and Engineering, University of Delaware, 201 DuPont Hall, Newark, DE 19716, United States
[b] Delaware Biotechnology Institute, 15 Innovation Way, Newark, DE 19711, United States
[c] Corporate Center for Analytical Sciences, DuPont Experimental Station, Wilmington, DE 19880, United States
[d] Department of Biomedical Research, Alfred I. Dupont Hospital for Children, 1600 Rockland Road, Wilmington, DE 19803, United States

ARTICLE INFO

Article history:
Received 28 March 2008
Received in revised form 5 June 2008
Accepted 6 June 2008
Available online 18 June 2008

Keywords:
Electrospinning
Poly(*N*-isopropyl acrylamide) (pNIPAM)
Spectroscopy

ABSTRACT

Poly(*N*-isopropyl acrylamide) (pNIPAM) is an interesting material in that it shows a thermoresponsive behavior around 32 °C in aqueous solutions. This behavior mimics that of many proteins in solution and as a result, many researchers have studied pNIPAM as a model for protein behavior. Yet, little is known about the processability of pNIPAM into three-dimensional matrices and whether such processing affects polymer conformation. In this work, 3D fibrous mats of pNIPAM were prepared by electrospinning from three different solvents and the resulting morphologies evaluated. Additionally, electrospun pNIPAM was evaluated with polarized Raman and infrared spectroscopies and compared against the spectra of the bulk material. It was found that the electrospinning process did not alter the polymer structure or morphology.

1. Introduction

Thermoresponsive poly(*N*-isopropyl acrylamide) (pNIPAM) has been well studied over the past 30 years. In aqueous solutions, pNIPAM has a lower critical solution temperature (LCST) in the range of 31–35 °C. Below the LCST, the polymer interacts readily with water; however, at temperatures above the LCST, entropic contributions to the polymer's free energy override enthalpic contributions, and it becomes energetically more favorable for the chains to condense on themselves. This phenomenon, often referred to as entropic union [1], results in the polymer precipitating out of aqueous solutions at temperatures above its LCST [2–4]. The LCST-associated phase transition of pNIPAM has been investigated using a variety of techniques including fluorescence polarization [5], light scattering [6], cloud point [7,8], turbidity [8], differential scanning calorimetry [8,9], infrared and Raman spectroscopies [9,10], and mathematical modeling [11]. In addition, it has been shown that the pNIPAM LCST can be increased or decreased with the addition of surfactants [12,13], salts [14], or additional solvents [15]. The alterability of pNIPAM LCST has allowed the development of several applications for the polymer including drug delivery [16–19], immunoseparation [20], biomaterials [21,22], cell culture [23], protein folding [24,25], radiotherapy [26], microactuators [27], sensors [28–32], catalysis, photonics, electronics, and optics [33,34].

Although pNIPAM has been extensively researched over the past few decades, it generally used as a gel in aqueous solutions, and the characteristics of fibrous pNIPAM are not well understood. In this work, pNIPAM was electrospun to create three-dimensional, solid state, fibrous mats that could be used as scaffolds, templates, or filters at high temperature and then easily removed at low temperature. Importantly, previous work by our group indicates that the electrospinning process can induce conformational changes in polymers, and it is critical to characterize polymers before and after processing [35–37]. To this end, we analyzed electrospun membranes of pNIPAM with polarized Raman and FT-IR spectroscopies. The work described here evaluates the electrospinnability of pNIPAM in three different solvents as well as solution viscosity and solid phase characterization.

2. Experimental

2.1. Materials

Poly(*N*-isopropyl acrylamide) with an approximate viscosity average molecular weight (M_v) of 300,000 Da was purchased from Scientific Polymer Products, Inc. (Ontario, NY) and used as-received. The solvents chosen for this research were cold deionized water, acetone, and tetrahydrofuran (THF). Solvents were purchased from Fisher Scientific (Fairlawn, NJ) and were also used as-received, with the exception of the deionized water that was

* Corresponding author. Department of Materials Science and Engineering, University of Delaware, 201 DuPont Hall, Newark, DE 19716, United States. Tel.: +1 3028314476; fax: +1 3028314545.
E-mail address: rabolt@udel.edu (J.F. Rabolt).

0032-3861/$ – see front matter © 2008 Elsevier Ltd. All rights reserved.
doi:10.1016/j.polymer.2008.06.018

used from an in-house line. Because each solvent interacted with the polymer differently, a series of concentrations were evaluated for each solvent system. For each system the concentration was increased in increments of 2 w/v% (weight/volume percentage) starting at 6–14, 6–18, and 12–18 w/v% for water, acetone, and THF, respectively.

2.2. Viscosity measurements

Solution viscosities were measured in triplicate with a BYK Gardner CAP 2000+ (Columbia, MD) viscometer. For each test, the stage was heated to 25 °C, the rotational speed was set to 100 rpm, and the shear rate was 333 Hz. A solvent trap was also used in order to limit the amount of solvent loss during the acquisition time.

2.3. Electrospinning

The electrospinning apparatus consisted of a variable syringe pump (Orion Sage, Thermo Scientific, Sugar Land, TX) and a high voltage supply (Glassman Series ED, High Bridge, NJ). A glass syringe (Popper & Sons, Inc., New Hyde Park, NY) was filled with the polymer solution and the needle gauge (Hamilton, Reno, NV) was selected so that the solution would flow out but not continuously drip when pressure was applied (see Table 1 for gauge selection). In order to commence electrospinning, the syringe was placed on the syringe pump; the pump was turned on to supply a continuous flow of solution to the tip, and a voltage of +10 kV was applied. The fibers were collected on a grounded collecting plate. Aligned samples were also collected to study polymer conformation. For the aligned samples, fibers were collected on either a grounded mandrel rotating at 2500 rpm (13.2 m/s) or on a charged plate (−5 kV) with a 1-in gap to induce the Hall Effect [38].

2.4. Imaging

Samples were imaged with both an optical microscope and a field emission scanning electron microscope (FE-SEM) to view macroscopic and microscopic features. For optical images, samples were collected directly onto glass slides during the electrospinning process. Images were taken on an Olympus BX60 (Center Valley, PA) fitted with a Panasonic CCTV camera (Secaucus, NJ).

FE-SEM measurements were carried out on a JOEL JSM 7400F (Tokyo, Japan). Samples were coated with 10 Å of gold/palladium (Denton Desk II, Moorestown, NJ) prior to imaging. Images were obtained at a working distance of 8 mm using an acceleration voltage of 1 kV.

2.5. Spectroscopy

Raman measurements were carried out using a Kaiser HoloPro spectrograph (Ann Arbor, MI) equipped with a Princeton Instruments CCD camera (Trenton, NJ). A Ti:Sapphire laser pumped by a frequency-doubled Nd:YAG laser and operating at 785 nm with a power between 50 and 100 mW (depending on sample requirements) was used as the excitation source. The laser light was incident on the sample and then backscattered at 180° to be collected by an f/1.8 collection lens. Fourier transform infrared spectroscopic (FT-IR) measurements were obtained utilizing a Thermo Nicolet Nexus 670 spectrometer. Both powdered and electrospun pNIPAMs were pressed into potassium bromide (KBr, Fisher Scientific) pellets prior to data collection.

Table 1
Needle gauges used for each concentration

Concentration (w/v%)	Water	Acetone	THF
6	26	30	
8	26	26	
10	26	26	
12	23	26	26
14	23	23	23
16		23	23
18		23	23

Inner diameter: 30 = 0.16 mm; 26 = 0.26 mm; 23 = 0.34 mm.

3. Results and discussion

Previous reports on electrospinning pNIPAM are limited but show that the polymer can be electrospun from DMF [39]. In the present work, pNIPAM was electrospun under three different solvent conditions, and the resulting mats were characterized to determine whether any conformational changes occurred during processing.

3.1. Electrospinnability

For each solvent system, the concentration of polymer in the solution will vary due to different interactions between the polymer and the solvent. Therefore, varying concentrations of pNIPAM were dissolved in water, acetone, or THF. The viscosity of each of the solutions was tested and then the samples were electrospun. As expected, as the concentration of polymer in solution was increased, viscosity also increased. Interestingly, the concentration-dependence of viscosity varied significantly across the different solvents. Fig. 1 shows the viscosity in poise (*P*) with respect to the weight per volume percent (w/v%) concentration of pNIPAM in solvent. Solutions in water exhibited considerably higher viscosities than solutions in either acetone or THF, even at lower pNIPAM concentrations. Concentrations from 6 to 14 w/v% pNIPAM in water showed viscosity increases from 1.3 to 6.0 P. In contrast, the viscosity of acetone solutions was so low at 6 w/v% pNIPAM in acetone that we could not accurately measure it, but viscosity increased from 0.9 to 2.5 P in the range of 8–18 w/v%. For THF, the trend was similar with viscosities increasing from 1.5 P at 12 w/v% to 3.2 P at 18 w/v%. Each of the systems studied showed a linear trend of increasing viscosity with increasing concentration.

As expected, pNIPAM fiber diameters also increased as the concentration of polymer increased in the solution. Fig. 2 shows average fiber diameters as a function of polymer concentration. The fibers spun from water had the smallest diameters ranging from 400 nm at the lowest concentration to 1.3 μ at the highest concentration. At 6 w/v% pNIPAM in acetone, the average fiber diameter of 600 nm was comparable to fibers spun from water at the

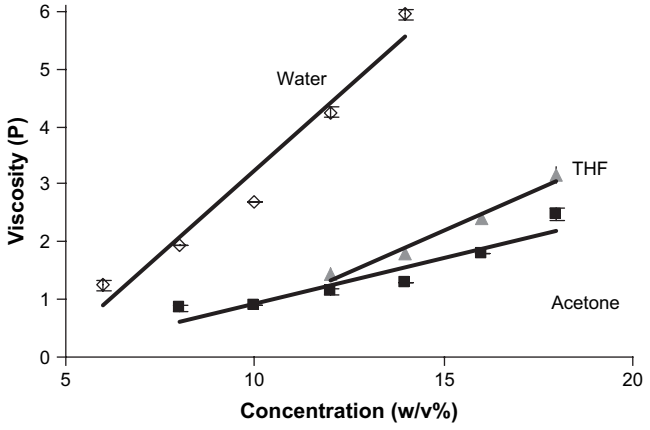

Fig. 1. Viscosity as a function of polymer concentration in solvent for solutions of pNIPAM in water (◇), THF (▲), and acetone (■).

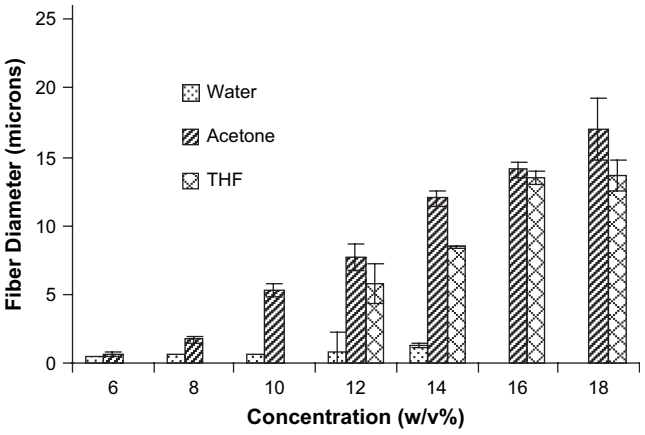

Fig. 2. Average fiber diameter as a function of concentration.

same concentration. As the concentration was increased though, the fibers spun from acetone dramatically increased in diameter with a final dimension of 17 μ at 18 w/v%. The fibers electrospun from THF also had larger diameters with a range from 5.8 to 13.6 μ as the concentration was increased from 12 to 18 w/v%.

The conformation of electrospun mats on FE-SEM imaging also changed with pNIPAM concentration. Fig. 3 shows images for five different concentrations of pNIPAM in water (6, 8, 10, 12, and 14 w/v%). At low concentrations, the fibers were sparse, and there was a prevalence of triangular formations. These triangular shapes appear like beads with short fibers at the corners. As the concentration was increased, the number of triangular beads began to decrease until only fibers were present at 12 w/v%. At this concentration, the average fiber diameter was 750 nm and the cross-section of the fibers appeared to be shaped like a narrow dog bone (see Fig. 6). Above 12 w/v%, the morphology of some of the fibers was distorted and aggregates of polymer were apparent. Therefore,

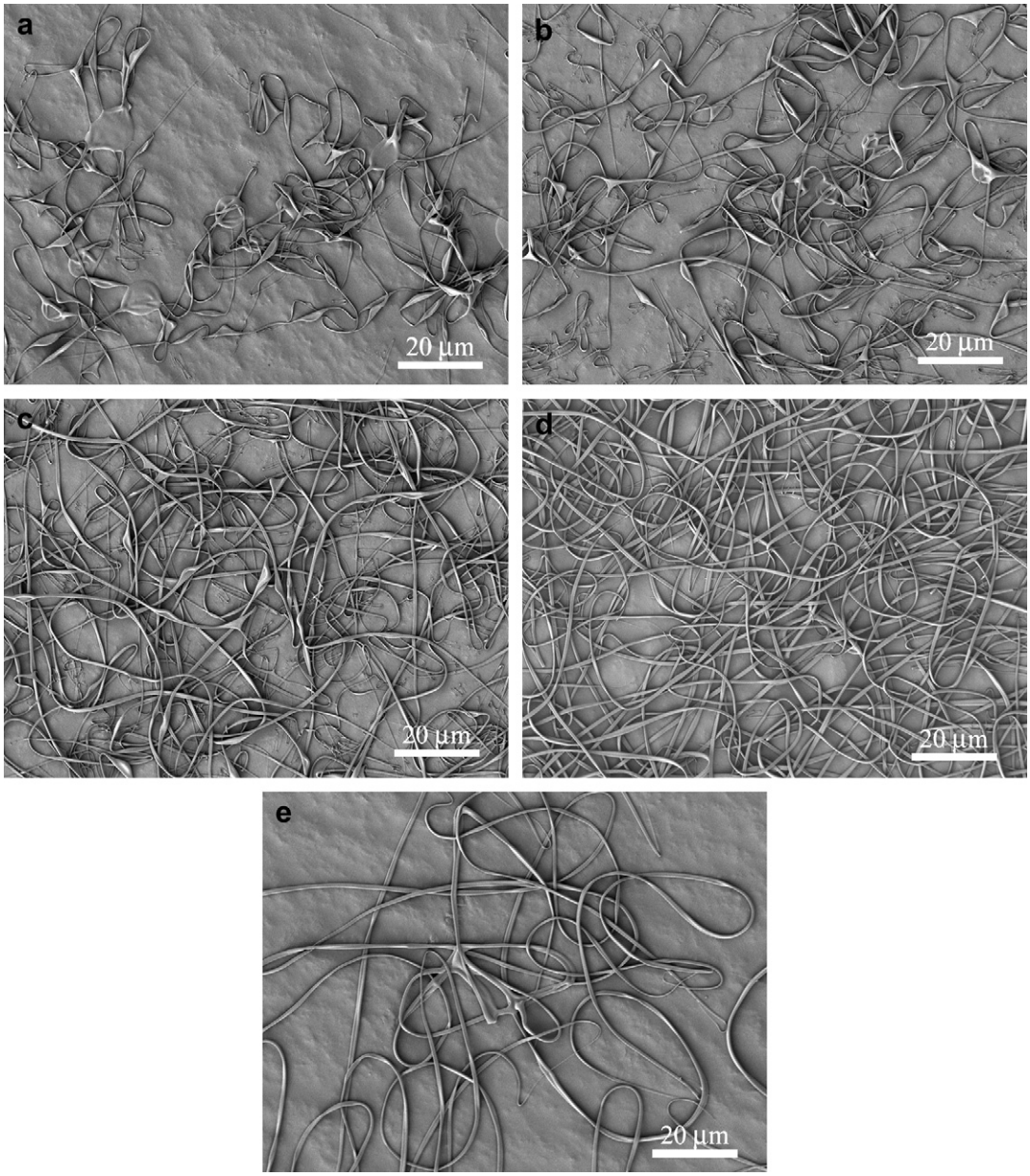

Fig. 3. FE-SEM micrographs of the concentration series for pNIPAM electrospun from water starting from the lowest concentration to the highest (a) 6, (b) 8, (c) 10, (d) 12, and (e) 14 w/v %. pNIPAM (12 w/v%) in water appears to produce the best fiber morphology with fairly uniform fibers and less triangular formations.

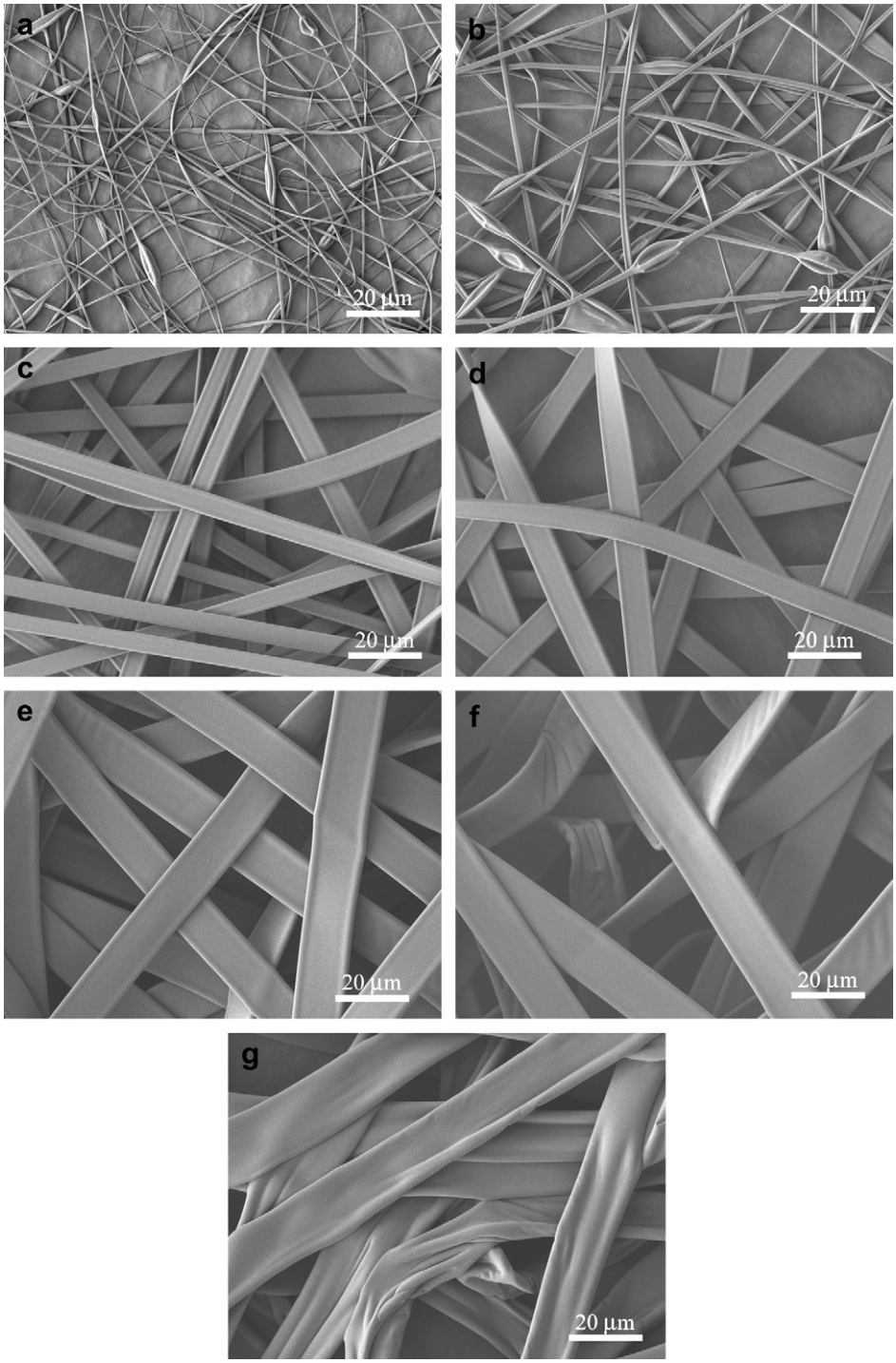

Fig. 4. FE-SEM micrographs of the concentration series for pNIPAM electrospun from acetone starting from the lowest concentration to the highest (a) 6, (b) 8, (c) 10, (d) 12, (e) 14, (f) 16, and (g) 18 w/v%. The range between 10 and 14 w/v% produces smooth fibers with increasing diameter as the concentration is increased, below this range fibers are beaded and above this range the morphology of the fibers is distorted.

we found that the optimal concentration for pNIPAM electrospun from water was 12 w/v%.

pNIPAM went into solution in acetone readily allowing a broader range of concentrations to be electrospun. Fig. 4 shows FE-SEM micrographs of pNIPAM spun from 6, 8, 10, 12, 14, 16, and 18 w/v% solutions. At lower concentrations (6 and 8 w/v%), the fibers had diameters of approximately 600 nm to 1.7 μm, respectively, with intermittent beads. At these concentrations, the cross-section of the fibers appeared to form the "narrow dog bone" shape (see Fig. 6) which is similar to pNIPAM spun from 12 w/v% water. As the concentration was increased, the distance between the ends of "dog bone" grew and the fibers turned into flat ribbons with rounded edges. Between 10 and 14 w/v%, the fibers exhibited this flat morphology and the width of the fibers increased steadily with the concentration. At 16 w/v%, surface corrugation became apparent where fibers bent; wrinkles were more prominent in membranes spun from the 18 w/v% solution. Therefore, the optimal concentration for electrospinning

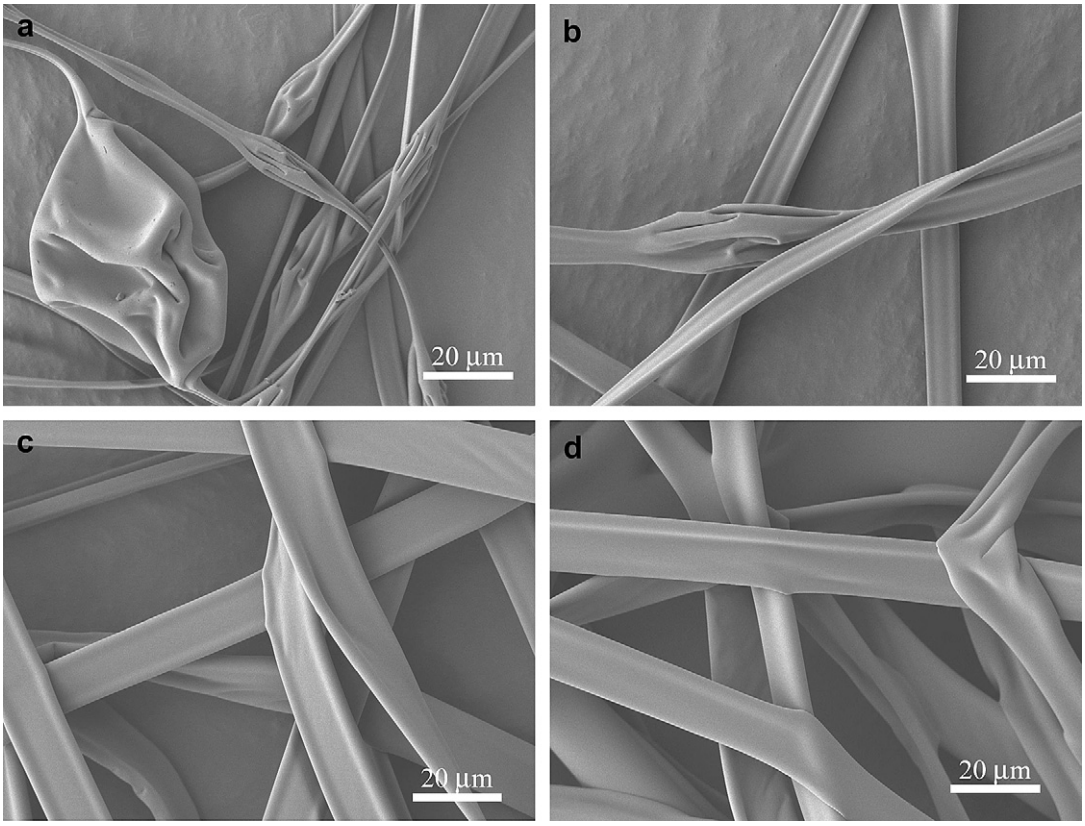

Fig. 5. FE-SEM micrographs of the concentration series for pNIPAM electrospun from THF starting from the lowest concentration to the highest (a) 12, (b) 14, (c) 16, and (d) 18 w/v%. At higher concentrations (20 and 22 w/v%, data not shown), the solutions were too viscous to electrospin and instead fibers were extruded from the needle.

pNIPAM fibers from acetone appears to be within the 10–14 w/v% range.

Fibers electrospun from THF had similar morphologies to those spun from acetone. Fig. 5 shows fibers electrospun from THF in concentrations of 12, 14, 16, and 18 w/v%. Once again, the transition from beaded fibers at low concentrations to uniform fibers at higher concentrations was observed. There was a much narrower concentration range for THF and we were only able to get actual fibers between 12 and 18 w/v%. Fibers spun from 12 and 14 w/v% exhibited a "beads-on-a-string" morphology, which was not apparent in fibers spun from 16 and 18 w/v% solutions. At 18 w/v%, the electrospun fibers appeared more wrinkled and adherent to each other and concentrations higher than 18 w/v% did not yield fibers but instead appeared to be extruded rather than electrospun (data not shown). Thus, the optimal electrospinning concentration for pNIPAM fibers spun from THF is 16 w/v%. At this concentration, the fibers have a "flat dog bone" cross-section (see Fig. 6) and the fiber widths were fairly uniform at 13.5 μm. Although the cross-sections of the fibers spun from both acetone and THF are similar, they differ in that the fibers from THF had larger diameters (13.5 μm for THF fibers versus 5.3–12 μm, depending on the concentration used, for acetone spun fibers). Additionally, the THF spun fibers often fused together at junction points.

Fig. 6. Graphical depictions of fiber cross-sections.

The morphology of electrospun fibers can be attributed to three main influences, including the surface tension of the jet, solution viscosity, and the net charge density carried by the jet [40,41]. Surface tension is influenced by the interaction between the polymer and the solvent; solution viscosity can be changed by varying the polymer in solution, and net charge density is primarily affected by the applied electric field. As the concentration of polymer is increased, therefore, the surface tension and solution viscosity are altered, and these influence the resulting fiber morphology. At lower concentrations, beaded fibers are formed when the number of chain entanglements is low. Fong et al. [40] describe the formation of beads as a state similar to the capillary break-up of droplets of a low molecular weight liquid during electrospraying. When the polymer has a higher molecular weight, a fiber between the beads is created to make the "beads-on-a-string". This is caused by the contraction of the jet due to surface tension. As the viscosity of the solution is increased, and subsequently the number of chain entanglements, the beads become bigger and more spaced out while the diameter of the fiber also increases. Eventually a beadless fiber is formed. In fibers with circular cross-sections, smooth, circular beads are often observed. In our system though, when pNIPAM was spun from THF or acetone, the surface of the beads was wrinkled. We hypothesize that the mechanism that drives the formation of these wrinkled beads is similar to the one that produces flat fibers. Reneker and co-workers proposed a theory for the formation of flat fibers in which a thin skin is formed on the electrospinning jet [41]. When the residual solvent inside the jet escapes, the atmospheric pressure collapses the tube to form a flat ribbon. Ribbons with thick edges were also observed and Reneker attributed this morphology to the distribution of electrical

charge to the edges of the fiber which therefore produced hollow tubes at the lateral edges of the fiber. Similarly, we believe that when beads form, they too have a thin skin. When the solvent diffuses out of the bead, it causes the shell to collapse leaving a wrinkled texture.

Wrinkling was also apparent on isotropic fibers spun at high concentrations. At these higher concentrations, there was less solvent to evaporate and therefore the fibers dried earlier than some of the lower concentration samples. It is our hypothesis that these thick, dry fibers landed on the flat substrate and bent under the force of gravity. Hence there is a wrinkled appearance on the fiber skin where it is bent or twisted as opposed to where it is lying flat.

3.2. Optical microscopy

Optical microscopy studies were performed to determine the fiber lengths of fibers that were too long to measure in the FE-SEM. In Fig. 7, fibers spun from 12 w/v% pNIPAM in water, 10 w/v% in acetone, and 16 w/v% in THF are shown. These are within the optimal conditions for each of the solvent systems. As indicated above, the average diameter of fibers formed under these conditions was 750 nm for water, 5.3 μm for acetone, and 13.5 μm for THF. The optical micrographs confirm these approximate fiber diameters, but it should be noted that fibers spun from water were only a few hundred microns long whereas fibers from acetone and THF extended outside the field of view. This result suggests that the electrospinning jet of the pNIPAM/water system could not withstand the whipping motion and instead, the jet broke to form short fibers.

A possible explanation for the observation that dramatically shorter fibers are spun from water is that water is only a moderate solvent for pNIPAM. The solubility parameter is 18.5 $MPa^{1/2}$ for THF [42] and 19.7 $MPa^{1/2}$ for acetone [42], while in contrast, the solubility parameter of water [42] is 48.0 $MPa^{1/2}$. The solubility parameter for pNIPAM can be calculated by the following equation [43],

$$\delta = \frac{\rho \sum G}{M} \quad (1)$$

where ρ is the density of the polymer (1.10 g/cm^3), G is the group molar attraction constant for each of the constituent chemical groups in the polymer, and M is the molecular weight of the mer (113 g/mol). The general rule that "like dissolves like" may apply, supporting the notion that water is a moderate solvent for pNIPAM; whereas, THF and acetone are good solvents. When a polymer chain is in a good solvent, it is extended and able to interact with other polymer chains. When a polymer is not in a good solvent, the macromolecule energetically favors itself over the solvent molecules and therefore the polymer chain folds into a sphere [44]. In this state, interactions with other chains are limited and therefore it is difficult to maintain a continuous jet during electrospinning. This could produce mechanically weak fibers that may fracture during spinning. Of course, the solubility parameter does not take into account the hydrogen bonding that is present in an aqueous solution so it is probable that the other factors are influencing the behavior of pNIPAM while it is being electrospun from water.

3.3. Polymer characterization

In order to determine if the electrospinning process caused any conformational changes to the polymer, the bulk and electrospun polymers were investigated with polarized Raman and FT-IR spectroscopies. Previous reports from our group [36,37] have shown that electrospinning can cause a change in the conformation of polymers including nylon and spider silk. Additionally, Kakade et al. [35] have shown that the macroscopic alignment of electrospun polyethylene oxide can induce molecular alignment along the primary axis of the fiber.

Fig. 8 shows the polarized Raman spectra of the bulk pNIPAM and the electrospun fibers. For the electrospun mat, the polarizer and analyzer were both set to the z position, choosing an arbitrary direction on the mat as "z", for one spectrum and then both changed to the y position for the second spectrum to detect the differences in molecular alignment, which would be indicated by intensity differences between the polarized spectra. The spectral bands were assigned as is shown in Table 2 [10,45]. The chemical structure of pNIPAM consists of an alkyl chain with a pendant chain extending from the backbone. This side group has a carbonyl, a tertiary amine, and terminates with an isopropyl group. The spectra have been offset for visual clarity but for the most part all

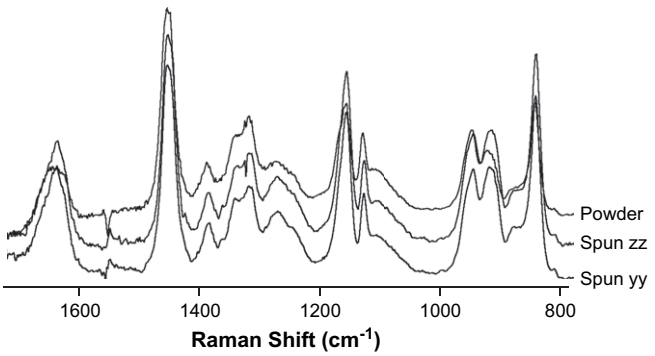

Fig. 8. Polarized Raman spectra of the bulk and electrospun pNIPAMs. Spectra were recorded with the polarizer and analyzer both in the z and then both in y positions for the isotropic spun pNIPAM in order to determine if there is any molecular alignment present.

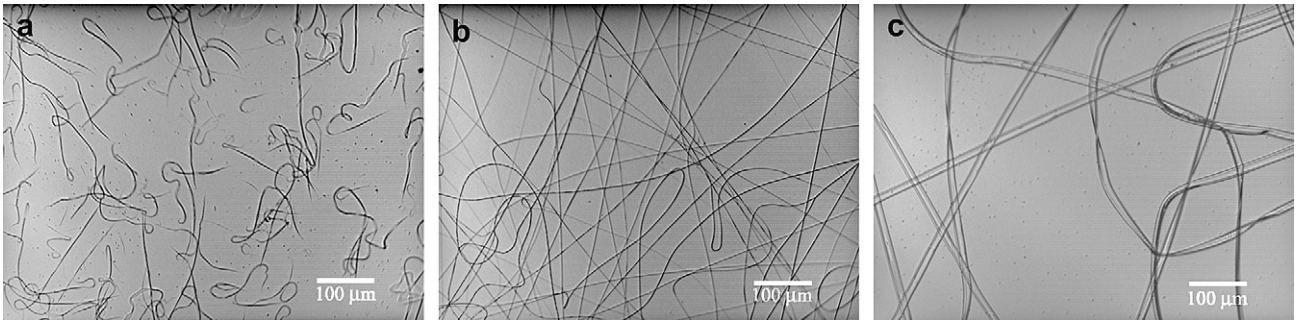

Fig. 7. Optical microscopic images of fibers taken at the optimal concentration for each of the solvent systems: (a) 12 w/v% pNIPAM/water, (b) 10 w/v% pNIPAM/acetone, and (c) 16 w/v% pNIPAM/THF. Images were taken with a 20× objective and the scale bar represents 100 μ.

Table 2
Identification of Raman shift and infrared band positions from Figs. 8 through 11 [10]

Raman Shift (cm^{-1})	IR Frequency (cm^{-1})	Assignment
845	840	CH_3 twist
	884	
921	928	CH_3 rock
949	984	CH_3 rock
1132	1131	C–C skeletal in-phase stretch
1160	1173	N–C bond stretch
	1245	
1277, 1317	1274, 1328	Doublet of overlapping C–N and C–H
	1368, 1388	Twin methyl
1388		CH_3 bend
1453	1460	CH_3 bend (scissors deformation)
1554	1548	Amide II N–H deformation
1642	1657	Amide I C=O stretch

three spectra were very similar. Most notably, the CH_3 twist (845 cm^{-1}), CH_3 rock (921 and 949 cm^{-1}), CC stretch (1132 cm^{-1}), NC stretch (1160 cm^{-1}), and the CH_3 scissor deformation (1453 cm^{-1}) were all moderately strong and exhibited similar relative intensities in each of the spectra. These results indicate that the process of electrospinning did not induce conformational changes to the polymer backbone since new bands or changes in relative intensities would have been observed.

In order to confirm that the alignment also did not alter the polymer conformation, aligned mats were spun by two different methods. The first employed a rotating mandrel that rotated at 2500 rpm and was grounded in order to attract the charged fibers. The second method is the induced alignment of the fibers by taking advantage of the Hall effect. Two metal bars were negatively charged in order to attract the positively charged fibers. In order to balance the charge repulsion, the fibers bridged the gap between the bars and formed an aligned mat. Both of these samples were analyzed with polarized Raman spectroscopy and their spectra are shown in Figs. 9 and 10. For both samples, the polarized spectra were identical, which indicates that the molecular alignment was not induced even in samples in which macroscopic alignment is present.

To more completely assess the molecular orientation of pNIPAM, the bulk powder and electrospun mats were also analyzed in the infrared region of the spectrum Fig. 11. It is important to analyze samples with both FT-IR and Raman spectroscopies because symmetric vibrations show more intense Raman scattering whereas absorption in the infrared regions is stronger for asymmetric vibrations. Sample preparation can be difficult for FT-IR measurements because the sample must be thin enough so that it is transparent to the IR beam. In addition, for the electrospun fibers,

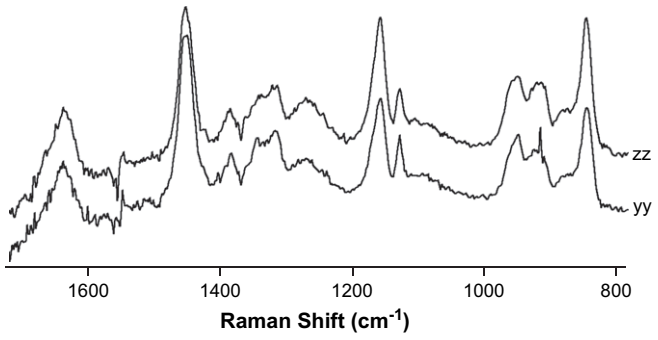

Fig. 9. Polarized Raman spectra of pNIPAM fibers aligned on a rotating mandrel (polarizer and analyzer at both at *z* and *y* positions for the respective spectra). Macroscopic alignment does not appear to cause molecular alignment.

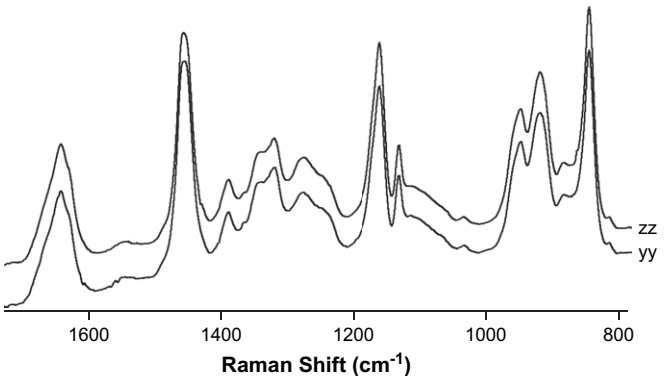

Fig. 10. Polarized Raman spectra of electrospun pNIPAM aligned using the Hall Effect (polarizer and analyzer at both at *z* and *y* positions for the respective spectra). Once again, no molecular alignment was evident.

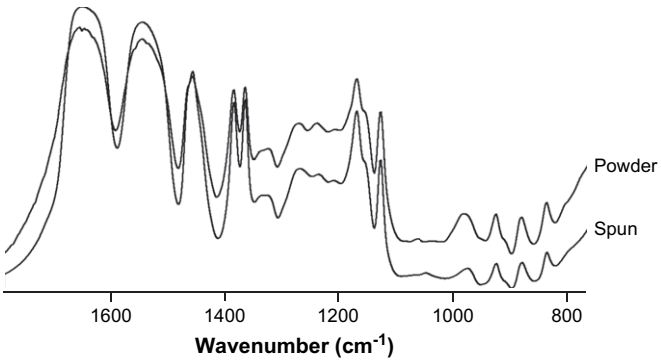

Fig. 11. FT-IR spectra of electrospun and powdered pNIPAMs.

the fiber diameters are on the same order of magnitude as the wavelength of the infrared light being used in the measurement. This causes interference and the texture of the mat scatters the IR radiation making it difficult to obtain spectral information from the resulting spectra. To overcome these limitations, both the bulk powder and the electrospun membranes were pressed into KBr pellets. For the bulk polymer, a low concentration of polymer (5 wt%) was present so that spectrum was not saturated. In the case of the electrospun mat, the KBr filled the voids in the mat and reduced the scattering. The peak assignments can be found from Table 2 [10]. The FT-IR data agree with the Raman analysis in that the process of electrospinning does not alter the polymer.

4. Conclusions

We have found that it is possible to electrospin pNIPAM into three-dimensional matrices and that the processing does not induce conformational changes within the polymer. When spun from water, pNIPAM formed small diameter fibers; however, these were of short length suggesting that the electrospinning jet was not able to withstand the whipping motion. In contrast, fibers spun from acetone or THF had diameters in the range of 5–17 μm. These were able to withstand the electrospinning process and were, therefore, able to produce non-woven, fibrous mats. We propose that the solubility parameter largely accounts for the ability of a continuous pNIPAM fiber to be electrospun from THF and acetone but not from water. Additionally, characterization with polarized Raman and FT-IR showed that electrospun mats of all types had identical chain structure when compared to the bulk polymer indicating that the

electrospinning process did not cause a change in conformational structure.

Acknowledgements

The authors would like to thank Dr. Chris Snively for useful conversations on infrared spectroscopy and additional thanks go to Frank Kriss and Dr. Chao Ni for assistance in electron microscopy. This work is funded through NSF-NIRT and NSF awards DMR – 0315461 and DMR – 0704970.

References

[1] Lauffer MA. Entropy-driven processes in biology: polymerization of tobacco mosaic virus protein and similar reactions, vol. 20. New York, Heidelberg, Berlin: Springer-Verlag; 1975. p. 264.
[2] Cheng X, Canavan HE, Stein MJ, Hull JR, Kweskin SJ, Wagner MS, et al. Langmuir 2005;21(17):7833–41.
[3] Graziano G. International Journal of Biological Macromolecules 2000;27(1):89–97.
[4] Li Y, Tanaka T. Journal of Chemical Physics 1989;90(9):5161–6.
[5] Binkert T, Oberreich J, Meewes M, Nyffenegger R, Ricka J. Macromolecules 1991;24(21):5806–10.
[6] Heskins M, Guillet JE. Journal of Macromolecular Science, Chemistry 1968;A2(8):1441–55.
[7] Matsuda Y, Miyazaki Y, Sugihara S, Aoshima S, Saito K, Sato T. Journal of Polymer Science, Part B: Polymer Physics 2005;43(20):2937–49.
[8] Boutris C, Chatzi EG, Kiparissides C. Polymer 1997;38(10):2567–70.
[9] Maeda Y, Higuchi T, Ikeda I. Langmuir 2001;17(24):7535–9.
[10] Lynch I, Blute IA, Zhmud B, MacArtain P, Tosetto M, Allen LT, et al. Chemistry of Materials 2005;17(15):3889–98.
[11] Okada Y, Tanaka F. Macromolecules 2005;38(10):4465–71.
[12] Ricka J, Meewes M, Nyffenegger R, Binkert T. Physical Review Letters 1990;65(5):657–60.
[13] Meewes M, Ricka J, Desilva M, Nyffenegger R, Binkert T. Macromolecules 1991;24(21):5811–6.
[14] Van Durme K, Rahier H, Van Mele B. Macromolecules 2005;38(24):10155–63.
[15] Winnik FM, Ringsdorf H, Venzmer J. Macromolecules 1990;23(8):2415–6.
[16] Nolan CM, Reyes CD, Debord JD, Garcia AJ, Lyon LA. Biomacromolecules 2005;6(4):2032–9.
[17] Lin CL, Chiu WY, Lee CF. Journal of Colloid and Interface Science 2005;290(2):397–405.
[18] Lo CL, Lin KM, Hsiue GH. Journal of Controlled Release 2005;104(3):477–88.
[19] Zhang JT, Huang SW, Zhuo RX. Macromolecular Bioscience 2004;4(6):575–8.
[20] Fong RB, Ding ZL, Hoffman AS, Stayton PS. Biotechnology and Bioengineering 2002;79(3):271–6.
[21] Sauzedde F, Elaissari A, Pichot C. Colloid and Polymer Science 1999;277(9):846–55.
[22] Liu L, Sheardown H. Biomaterials 2005;26(3):233–44.
[23] Shimizu T, Yamato M, Isoi Y, Akutsu T, Setomaru T, Abe K, et al. Circulation Research 2002;90(3):e40–8.
[24] Lu DN, Liu Z. Acta Polymerica Sinica 2004;4:573–9.
[25] Cui ZF, Guan YX, Yao SJ. Chinese Journal of Chemical Engineering 2004;12(4):556–60.
[26] Hruby M, Subr V, Kucka J, Kozempel J, Lebeda O, Sikora A. Applied Radiation and Isotopes 2005;63(4):423–31.
[27] Luo QZ, Mutlu S, Gianchandani YB, Svec F, Frechet JMJ. Electrophoresis 2003;24(21):3694–702.
[28] Suzuki D, Kawaguchi H. Langmuir 2005;21(18):8175–9.
[29] Wang ZH, Kuckling D, Johannsmann D. Soft Materials 2003;1(3):353–64.
[30] Roy I, Gupta MN. Chemistry and Biology 2003;10(12):1161–71.
[31] Cheng XH, Wang YB, Hanein Y, Bohringer KF, Ratner BD. Journal of Biomedical Materials Research Part A 2004;70A(2):159–68.
[32] Hoare T, Pelton R. Macromolecules 2004;37(7):2544–50.
[33] Wang C, Flynn NT, Langer R. Advanced Materials 2004;16(13):1074–9.
[34] Weissman JM, Sunkara HB, Tse AS, Asher SA. Science 1996;274(5289):959–60.
[35] Kakade MV, Givens S, Gardner K, Lee KH, Chase DB, Rabolt JF. Journal of the American Chemical Society 2007;129(10):2777–82.
[36] Stephens JS, Chase DB, Rabolt JF. Macromolecules 2004;37:877–81.
[37] Stephens JS, Fahnestock SR, Farmer RS, Kiick KL, Chase DB, Rabolt JF. Biomacromolecules 2005;6(3):1405–13.
[38] Li D, Wang Y, Xia Y. Nano Letters 2003;3(8):1167–71.
[39] Chen H, Hsieh YL. Journal of Polymer Science, Part A: Polymer Chemistry 2004;42(24):6331–9.
[40] Fong H, Chun I, Reneker DH. Polymer 1999;40:4585–92.
[41] Yarin AL, Koombhongse S, Reneker DH. Journal of Applied Physics 2001;89(5):3018–26.
[42] Plasticsusa.com. Solubility parameter of polymers and solvents. Available from: www.plasticsusa.com/solub.html; 21 February, 2006.
[43] Sperling LH. Introduction to physical polymer science. 3rd ed. New York: Wiley-Interscience; 2001. p. 671.
[44] Rubinstein M, Colby RH. Polymer physics. Oxford: Oxford University Press; 2003. p. 440.
[45] Zeng F, Tong Z, Yang XZ. European Polymer Journal 1997;33(9):1553–6.